

Manuscript Number: CARBPOL-D-19-00962R3

Title: Chitosan/glycosaminoglycan scaffolds for skin reparation

Article Type: Research Paper

Keywords: electrospinning; chitosan; chondroitin sulfate; hyaluronic acid; chronic wound and burn healing; in vitro and in vivo models

Corresponding Author: Professor Giuseppina Sandri, PhD

Corresponding Author's Institution: University of Pavia

First Author: Giuseppina Sandri, PhD

Order of Authors: Giuseppina Sandri, PhD; Silvia Rossi; Maria Cristina Bonferoni; Dalila Miele; Angela Faccendini; Elena Del Favero; Emanuela Di Cola; Antonia Icaro Cornaglia; Cinzia Boselli; Thomas Luxbacher; Lorenzo Malavasi; Laura Cantù; Franca Ferrari

Abstract: Burns and chronic wounds, often related to chronic diseases (as diabetes and cancer), are challenging lesions, difficult to heal. The prompt and full reconstitution of a functional skin is at the basis of the development of biopolymer-based scaffolds, representing a 3D substrate mimicking the dermal extracellular matrix. Aim of the work was to develop scaffolds intended for skin regeneration, according to: fabrication by electrospinning from aqueous polysaccharide solutions; prompt and easy treatment to obtain scaffolds insoluble in aqueous fluids; best performance in supporting wound healing. Three formulations were tested, based on chitosan (CH) and pullulan (P), associated with glycosaminoglycans (chondroitin sulfate - CS or hyaluronic acid - HA). A multidisciplinary approach has been used: chemico-physical characterization and preclinical evaluation allowed to obtain integrated information. This supports that CS gives distinctive properties and optimal features to the scaffold structure for promoting cell proliferation leading tissue reparation towards a complete skin restore.

Research Data Related to this Submission

There are no linked research data sets for this submission. The following reason is given:

Data will be made available on request

Highlights

Electrospun chitosan/glycosaminoglycan scaffolds for skin reparation were developed.

The scaffolds were insoluble in aqueous fluids after crosslinking by heating.

Chondroitin sulfate renders the scaffold best suited to heal lesions in murine model.

Chondroitin sulfate provides system flexibility for optimal preclinical performance.

1 Chitosan/glycosaminoglycan scaffolds for skin reparation

2

3 Giuseppina Sandri^{1,*}, Silvia Rossi¹, Maria Cristina Bonferoni¹, Dalila Miele¹, Angela Faccendini¹, Elena Del

4 Favero², Emanuela Di Cola², Antonia Icaro Cornaglia³, Cinzia Boselli¹, Thomas Luxbacher⁴, Lorenzo

5 Malavasi⁵, Laura Cantu^{2,*}, Franca Ferrari¹

6

7 ¹Department of Drug Sciences, University of Pavia, Viale Taramelli 12, 27100 Pavia, Italy

8 ²Department of Medical Biotechnology and Translational Medicine, University of Milano, LITA, Via Fratelli

9 Cervi 93, 20090 Segrate (Milano) Italy

10 ³Department of Public Health, Experimental and Forensic Medicine, University of Pavia, via Forlanini 2,

11 27100 Pavia, Italy

12 ⁴Anton Paar GmbH, Anton-Paar-Str, 20 8054 Graz, Austria

13 ⁵Department of Chemistry, University of Pavia, Viale Taramelli 14, 27100 Pavia, Italy

14

15 *Corresponding authors:

16 Prof. Giuseppina Sandri

17 Department of Drug Sciences,

18 University of Pavia,

19 Viale Taramelli 12, 27100 Pavia, Italy

20 giuseppina.sandri@unipv.it

21

22 Prof. Cantu' Laura

23 Department of Medical Biotechnology and Translational Medicine

24 University of Milano

25 LITA, Via Fratelli Cervi 93, 20090 Segrate, Italy

26 laura.cantu@unimi.it

27

28 ABSTRACT

29 Burns and chronic wounds, often related to chronic diseases (as diabetes and cancer), are challenging
30 lesions, difficult to heal. The prompt and full reconstitution of a functional skin is at the basis of the
31 development of biopolymer-based scaffolds, representing a 3D substrate mimicking the dermal extracellular
32 matrix. Aim of the work was to develop scaffolds intended for skin regeneration, according to: fabrication by
33 electrospinning from aqueous polysaccharide solutions; prompt and easy treatment to obtain scaffolds
34 insoluble in aqueous fluids; best performance in supporting wound healing. Three formulations were tested,
35 based on chitosan (CH) and pullulan (P), associated with glycosaminoglycans (chondroitin sulfate - CS or
36 hyaluronic acid – HA). A multidisciplinary approach has been used: chemico-physical characterization and
37 preclinical evaluation allowed to obtain integrated information. This supports that CS gives distinctive
38 properties and optimal features to the scaffold structure for promoting cell proliferation leading tissue
39 reparation towards a complete skin restore.

40

41 Keywords: electrospinning, chitosan, glycosaminoglycans, chronic wound and burn healing, in vitro and in
42 vivo models

43

44 1. INTRODUCTION

45 Millions of people in the world suffer from chronic skin lesions. These are challenging and are affected by an
46 intrinsic inability to heal. Cellular and molecular abnormalities occurring at wound bed, including phenotypic
47 aberrations and perturbations of ECM microenvironment, significantly alter the normal recovery phases,
48 leading to a possible impairment of the healing path and finally to non-healing wounds. Moreover, among
49 skin wounds, burns require special attention because often prone to infections and to abnormal scarring
50 (Mafazzal Jahromi et al., 2018).

51 Because of the crucial barrier role of the skin, chronic wounds (including venous leg ulcers, diabetic foot
52 ulcers, arterial insufficiency and pressure ulcers) and burns impose substantial morbidity and mortality. They
53 deeply affect the quality of life of patients, with high economic burden (Stejskalova, Almquist, 2017).

54 Wound healing can be enhanced by tissue engineering: in particular, the use of scaffolds promotes the
55 formation of a defined biomimetic environment surrounding cells to allow cell-cell specific interactions
56 (Goldberg, Langer, Jia, 2012). The structure and morphology of the ECM of skin dermis can be easily
57 resembled by nanofibrous structures, reported as ideal constructs to enhance cell adhesion and proliferation
58 (Liu et al., 2017). Uniform and continuous nanofibers are easily obtained by means of electrospinning as a
59 simple, flexible and versatile method.

60 Given these premises, the aim of this work was the development of electrospun nanofibrous scaffolds based
61 on glycosaminoglycans, either chondroitin sulfate (CS) or hyaluronic acid (HA), and chitosan (CH), to
62 enhance cutaneous wound healing of chronic lesions and burns.

63 Glycosaminoglycans (GAGs) have been selected as important components of ECM and play a crucial role in
64 different stages of skin tissue regeneration and maturation. In particular CS, a structural component of ECM
65 (Oliveira, Reis, 2011) is able to interact with positively charged bioactive molecules, in particular growth
66 factors (GF) and is reported as effective enhancer of cell proliferation (Sandri et al., 2012; Sandri et al., 2015;
67 Sandri et al., 2016; Saporito et al., 2018). Analogously, HA plays pivotal roles in regulating proliferation,
68 migration, cell differentiation and angiogenesis (Kin et al., 2017).

69 Moreover CH has been selected as enabling polymer characterized by bioadhesion, biocompatibility,
70 biodegradability, antimicrobial activity, and wound healing properties (Liu et al., 2018).

71 However polysaccharides, in general, and CH, in particular, are hardly spinnable and CH nanofibers are
72 usually obtained starting from organic solution (i.e. trifluoacetic acid and hexa-fluoro isopropanol) that could
73 leave highly toxic traces or by blending chitosan with easily spinnable synthetic polymers (as poly(ethylene
74 oxide) or poly(vinyl alcohol) (Qasim et al., 2018).

75 In the present work, CH was associated to pullulan (P), an easily spinnable polysaccharide having numerous
 76 food, pharmaceutical and biomedical application (Singh et al., 2017). The preparation was robust with a one
 77 step process and easy to set up. An aqueous/acetic acid medium was used to avoid toxic residues and to
 78 allow the electrospinning of polymers having opposite charges (CH cationic and GAG anionic). Moreover,
 79 citric acid (CA) was used as crosslinker and a thermal treatment was applied to render the scaffold insoluble
 80 in aqueous environment. A multidisciplinary approach, involving chemico-physical and preclinical evaluation,
 81 has been used to characterize the scaffolds.

82

83 2. EXPERIMENTAL SECTION

84 2.1 Materials

85 Chitosan (CH) (charge density - positive = 0.006 mol/g), Chondroitin sodium sulfate (CS) (charge density -
 86 negative = 0.002 mol/g), Hyaluronic Acid (HA) (charge density - negative = 0.0013 mol/g) Pullulan (P) and
 87 citric acid (CA) (charge density - negative = 0.014 mol/g) were used (details summarized in supplementary
 88 information (SI), Fig. S1).

89 2.2. Methods

90 2.2.1. Preparation of polymeric blends and characterizations

91 All the polymeric blends were based on P, CH and CA, as such or containing CS or HA. P solution was
 92 prepared in distilled water and CS or HA were added to P, thus preparing three different solutions: P; P/CS
 93 P/HA. CH was hydrated in acetic acid (90% v/v) and citric acid was added. Three different polymeric blends
 94 were prepared by mixing each P, P/CS, and P/HA with CH solution at 1:1 weight ratio. The following blends
 95 were prepared (w/w): CH, CH/CS and CH/HA. The role of acetic acid was fundamental to reduce blend
 96 surface tension and allow their electrospinning. The blends composition is reported in Table 1.

97

98 Table 1: composition (% w/w) of polymeric blends used to be elctrospun for scaffolds construction. In the
 99 brackets the relative charge density per each component is reported.

% w/w	P	CH	CA	CS	HA	Water/acetic acid
CH	10	2.5 (+0.0015)	2.5 (-0.01)	--	--	55/45
CH/CS	10	2.5 (+0.0015)	2.5 (-0.01)	0.5 (-0.001)	--	55/45
CH/HA	10	2.5 (+0.0015)	2.5 (-0.01)	--	0.5 (-0.00065)	55/45

100

101 2.2.2. Physical properties of polymeric blends

102 The viscosity of CH, CH/CS and CH/HA blends was assessed by a rotational rheometer (Rheostress 600,
103 Haake, Enco, I), in the cone-plate configuration (C35/1: diameter= 35mm; cone angle= 1°), rest time = 3 min,
104 shear rate = 100 s⁻¹, T=25°C,

105 The surface tension of the blends was measured at T=32°C with a tensiometer (DY-300, Kyowa, J)
106 (measurement range 0-100 mN/m) and their electrical conductivity was determined by a conductometer
107 (FiveGoTM - Mettler Toledo, I).

108

109 2.2.3 Preparation of electrospun scaffolds

110 Scaffolds were obtained from the CH, CH/CS and CH/HA blends using an electrospinning apparatus (STKIT-
111 40, Linari Engineering, I), equipped with a high-voltage power supply (Razel R99-E 40, kV), a 10 ml syringe
112 with 21G needle (0.8x20 mm), and a conductive static collector, covered by an aluminum foil. The following
113 parameters were used: ΔV (voltage) = 21 kV (CH) or 15 kV (CH/CS and CH/HA), needle-to-collector
114 distance = 20 cm (CH) or 15 cm (CH/CS and CH/HA), polymeric solution flux = 0.4 ml/h, spinning time = 1 h.
115 The obtained CH, CH/CS and CH/HA scaffolds were then crosslinked by heating at 150°C for 1 h. This
116 process is also reported as able to dry sterilize the products (Kupiec et al., 2000).

117

118 2.2.3.1. Scaffold chemico-physical characterization

119 Scaffold morphology was analyzed by means of SEM (Tescan, Mira3XMU, CISRIC, University of Pavia) after
120 graphite sputtering. The scaffolds were analyzed before and after the crosslinking procedure and after 1-
121 week of hydration in distilled water. Nanofiber diameters were determined by an image analysis software
122 (Image J, ICY, Institute Pasteur, F).

123 FT-IR analysis was carried out by means of Infrared Imaging Microscope (Nicolet iN10 MX, Thermo
124 Scientific). The infrared spectra were acquired in the range 4000-500 cm⁻¹ (tested area 10-20 μm²).

125

126 2.2.3.2. Structural characterization

127 X-ray scattering experiments were performed at the high-brilliance ID02 beamline at ESRF (Grenoble,
128 France) in the q-ranges 0.007 ≤ q ≤ 5 nm⁻¹ (SAXS, mesoscale structure determination) and 15-30 nm⁻¹
129 (WAXS, local lengthscale organization). Small pieces (~1 cm²) were cut from the different scaffolds, both
130 before and after crosslinking. Cuts of the crosslinked membranes were dipped in distilled water or NaCl 156
131 mM solution 24 h before measurement. Both dry and wet samples were loaded in plastic capillaries 2 mm

132 thick (KI-beam, ENKI) and placed in front of the X-ray beam (Fig. S2a in SI). During data reduction, cell
133 contributions were subtracted from the measured spectra.

134

135 2.2.3.3 Calorimetry.

136 Small portions of different dry membranes (ranging 7-8 mg) either crosslinked or not, were adapted to
137 calibrated aluminum crucibles, then weighted. Crucibles were put into a solid state calorimeter (DSC131,
138 Setaram, FR), under nitrogen atmosphere, then submitted to subsequent temperature heating/cooling scans
139 at 2 °C/min or 10 °C/min scan rate in the temperature range 30-180°C, to test for process reversibility and
140 reproducibility. For the non-crosslinked samples, the first heating scan was limited to 150°C, then followed by
141 1h-isothermal equilibration at 150°C, similarly to the crosslinking protocol. Samples were equilibrated for 30
142 min at the extreme temperatures in between the subsequent scans. The background contribution of void
143 crucible was measured for subtraction and calibration.

144

145 2.2.3.4. Surface zeta potential

146 The apparent zeta potential (ζ) of each scaffold was determined from the measurement of the streaming
147 potential. Also, the streaming current was measured to estimate the extent of scaffold swelling affecting the
148 overall conductivity (see SI). Streaming potential measurements were performed with SurPASS™ 3 (Anton
149 Paar GmbH, Austria) using the clamping cell (Walker et al., 2002). The scaffolds (17x17 mm², active area
150 10x10 mm²) were mounted dry opposite to a reference surface (Figure S3a, SI).

151 10 mM KCl aqueous solution was used as the streaming solvent and its pH was scanned in the range 2.5-9,
152 to determine the isoelectric point (iep) and the ζ at physiological pH.

153 The ζ was calculated from streaming potential and streaming current measurements using the equations by
154 Helmholtz and von Smoluchowski (Luxbacher, 2014), as detailed in the SI. The contribution of the reference
155 material to the ζ of the scaffolds was estimated as negligible and the pH dependence of the ζ for these rigid,
156 non-porous, non-conductive materials is shown in SI (Fig. S3b).

157

158 2.2.3.5. Mechanical properties

159 Dried or hydrated scaffolds were subjected to tensile measurements by means of a TA.XT plus apparatus
160 (Stable Microsystems, ENCO, Italy), as briefly described in SI (Saporito et al., 2018a). The ratio between the
161 increase in the distance of the two grips at scaffold breaking and the initial one was then expressed in terms
162 of percent elongation of the scaffold, namely, $E\% = 100 \times (L_{fin} - L_{in}) / L_{in}$.

163

164 2.2.3.6. In vitro cells adhesion and proliferation assay

165 Adhesion and proliferation assays were carried out using two cell lines: fibroblasts (normal human dermal
166 fibroblasts (NHDF from juvenile foreskin, PromoCell, WVR, Italy) and endothelial cells from human umbilical
167 vein (HUVEC, Lonza, Italy), as briefly described in SI (Saporito et al., 2018a).

168 Scaffolds were cut to have a final area of 0.36 cm² (0.7 cm diameter) to cover the bottom of a 96 well-plate
169 and both cell types were seeded onto each scaffold at 10⁵ cells/cm² seeding density and grown for 3 and 6
170 days. Cells grown in standard conditions were considered as control (GM). After 3 or 6 days of growth, MTT
171 assay (as briefly described in SI (Sandri et al., 2017)), SEM and CLSM analysis (as briefly described in SI
172 (Saporito et al., 2018a)) were performed.

173

174 2.2.3.7. In vivo wound healing efficacy in murine burn/excisional model

175 All animal experiments were carried out in full compliance with the standard international ethical guidelines
176 (European Communities Council Directive 86/609/EEC) approved by Italian Health Ministry (D.L. 116/92).

177 The protocol is briefly reported in SI (Sandri et al., 2017). CH, CH/CS or CH/HA scaffolds having 4 mm
178 diameter as the lesions were applied and wetted with 20 µl of saline solution (0.9 g/l). Size of wounded area
179 and the histology of biopsies were performed, as briefly described in SI (Sandri et al., 2017).

180

181 2.2.3.8. Statistical analysis

182 Statistical differences were evaluated by means of a non-parametric test: Mann Whitney (Wilcoxon) W test,
183 (Statgraphics Centurion XV, Statistical Graphics Corporation, MD, USA). Differences were considered
184 significant at p<0.05.

185

186 3. Results and discussion

187 3.1. Physical properties of polymeric blends

188 The addition of CH-CA, alone and with CS or HA, significantly increased (~ one order of magnitude) the
189 viscosity of the solution as compared to pure P, as expected for molecular complexation. Then, the viscosity
190 values of the various blends are similar (within 3%), the smallest being that of CH/CS, compatible with a
191 more pronounced charge unbalance due to CS. The values of surface tension are almost similar for all
192 blends, the one of CH/CS being the lowest, again compatible with a more pronounced overall charge.

193 Accordingly, conductivity decreases in the series CH/CS>CH>CH/HA, with an overall span of ~20%. In fact

194 conductivity is directly related to the particle concentration and mobility in the solution. Unbalanced particle
195 charge density generally increases with the conductivity, influencing fiber diameter during electrospinning
196 (Huan et al., 2015). Table S1 (SI) reports the viscosity, surface tension and conductivity of the polymeric
197 blends used to prepare the scaffolds.

198

199 3.2. Scaffold chemico-physical and structural characterization

200 Different physico-chemical techniques were applied to assess the morphology and structure of the scaffolds
201 on different lengthscales. Besides the characterization of the final membranes, the effect of crosslinking was
202 addressed. In fact, while non-crosslinked membranes readily dissolve in contact with water, crosslinking
203 made them stable against solubilization. Moreover, the extent of scaffold stability was inspected by delayed
204 testing, as detailed in the following.

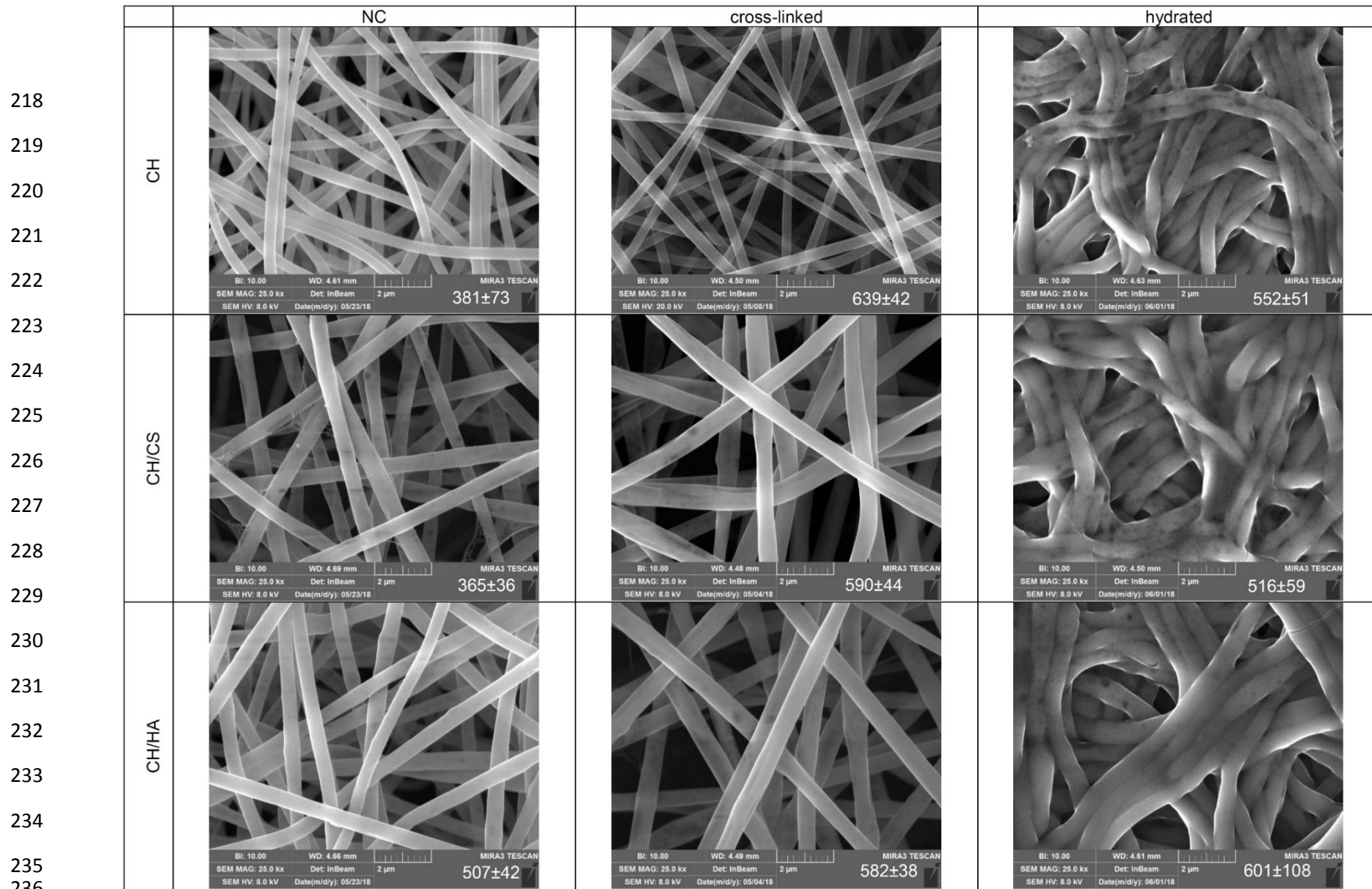
205

206 3.2.1. Fiber morphology

207 Figure 1 reports SEM microphotographs of nanofibrous scaffolds 1) immediately after preparation (not
208 crosslinked, NC, left), 2) after cross-linking (center) and 3) dried after 6 days immersion in water (right).
209 For all the compositions, nanofibers show regular shape and smooth surface and the cross-linking process
210 does not change their morphology. The regular and smooth appearance of nanofibers is preserved upon 6-
211 days hydration, although they show up to be stuck to each other.

212 The fibers cross section seems not to be altered upon crosslinking, being in the range of 500 nm in diameter,
213 nor they break in shorter tracts. In the CH scaffold the nanofibers are slightly thinner. Hydration causes a
214 slight swelling of the nanofibers, more evident in the CH scaffold and negligible in CH/CS. The wet fibers
215 morphology suggests that water penetration within the structure is not prevented for any of the compositions,
216 but that especially the CH/CS scaffold is more resistant against the fiber swelling deformation.

217



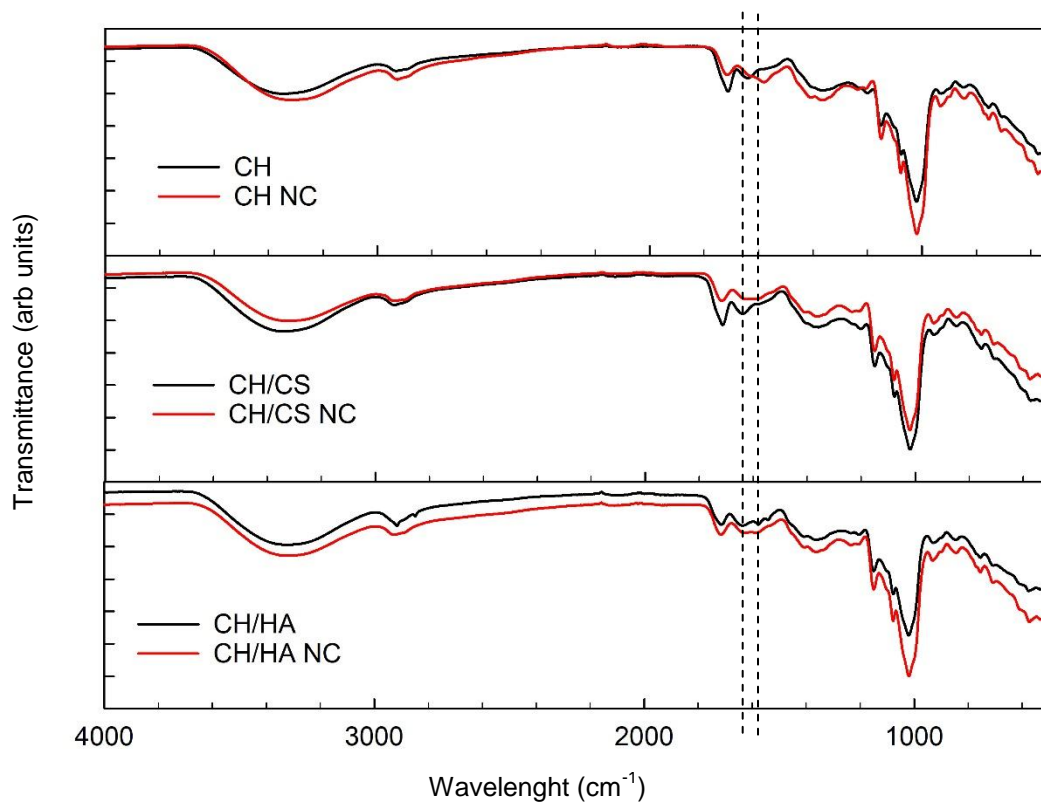
237 FIGURE 1: SEM microphotographs of scaffolds immediately after preparation (not crosslinked, NC), after cross-linking and after 6 days hydration in water. In
 238 each image the diameters (nm) are reported (mean values±sd; n=100) (Mann-Whitney – Wilcoxon: CH= NC vs hydrated: p=0.002; cross-linked vs hydrated:
 239 p=0.005; CH/HA: cross-linked vs hydrated: p=0.037; cross-linked: CH vs CH/CS: p=0.005; CH vs CH/HA: p=0.001; CH/CS vs CH/HA: p=0.018; hydrated: CH vs
 240 CH/CS: p=0.017; CH vs CH/HA: p=0.039)

241 Since, during the electrospinning and the subsequent crosslinking process, acetic acid volatilizes, it is
242 conceivable that anionic and cationic moieties could interact during this phase. Considering that CS is an
243 acid stronger than HA (pKa CS: 1.5-2; HA: 2.87), a tighter and stronger anionic/cationic interaction between
244 CS and CH could be at the basis of this behavior. although, in all systems, P forms mass-predominant
245 neutral matrix in a network formed by the interacting charged components with a clear excess of negative
246 charges (Table 1). It is conceivable that CH and CS or HA interacted forming polyelectrolyte complexes
247 (PEC) (Saporito et al., 2018b) and PEC could also occur, mediated by the CA macroion as crosslinker, since
248 CH polycation and CA multivalent macro-anion are present in the same weight fraction. The tuning
249 contribution coming from either HA or CS polyanions, present in lower amount in the corresponding
250 scaffolds, causes significant differences in swelling behavior.

251

252 3.2.2. FTIR characterization.

253 Figure 2 reports the FTIR profiles of the three scaffolds before and after crosslinking, giving a fiber local
254 response to crosslinking. Overall, the spectra are in agreement with current literature where the specific peak
255 assignment can be found (Harish Prashanth, Kittur and Tharanathan, 2002; Feng, Liu, Zhao and Hu, 2012).
256 As for CH scaffold, a significative effect following crosslinking is present in the region around 1640 cm^{-1} ,
257 typical of the Amide I band, that could be related to covalent bonds occurring between chitosan aminogroups
258 and carboxylic moieties of citric acid. For the two scaffolds CH/CS and CH/HA, differences are less marked
259 and only slight variations could be seen, again, in the region of Amide I band, suggesting that the presence
260 of anionic groups from CS (sulfate) and HA (carboxylic) and polymer steric hindrance could tune covalent
261 bond formation between CH and CA.



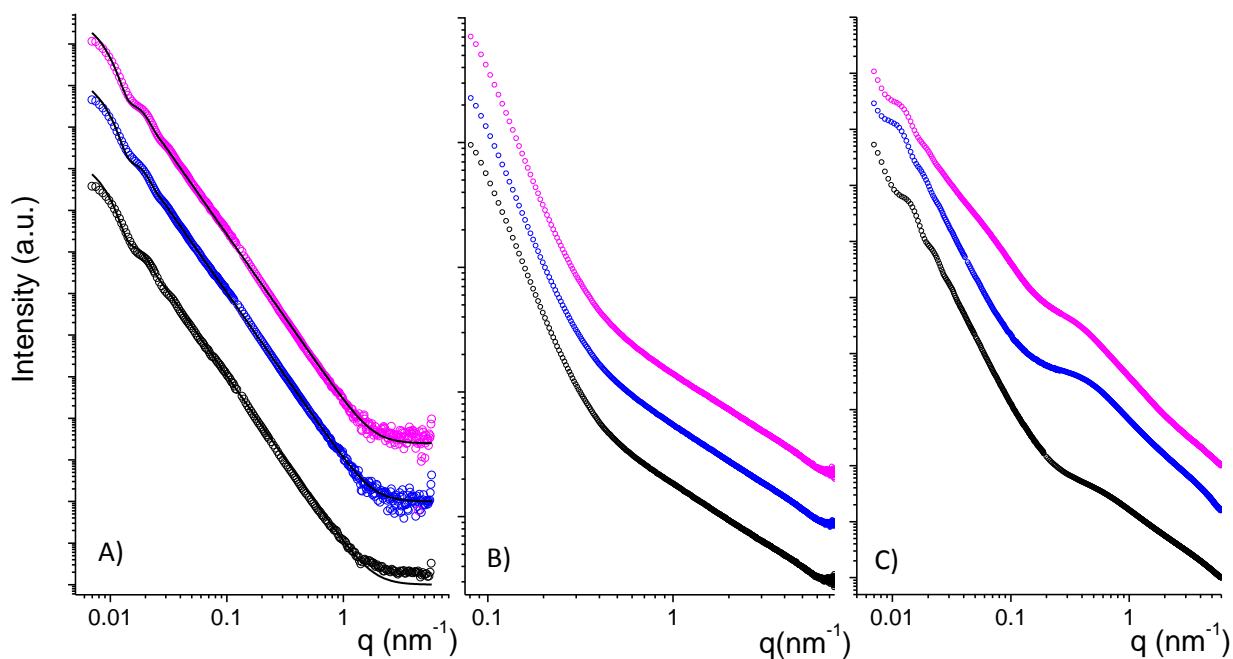
262

263 FIGURE 2: FTIR profiles for CH, CH/CS and CH/HA scaffolds, not crosslinked (NC) and crosslinked. A
 264 vertical dashed line is drawn in the region of the Amide I band.

265

266 3.2.3. Structural characterization

267 X-ray scattering measurements allow to access the structural features of the membranes from the
 268 mesoscale (SAXS, up to hundreds of nm) to the local arrangement (WAXS, down to tenth of nm), thus
 269 integrating the SEM morphological observation in revealing intra-fiber and inter-fiber structure, whether
 270 structural modification follow crosslinking, and hydration and aging effects. WAXS spectra in dry state does
 271 not display any feature for any of the membranes in any condition, thus showing that the electrospun blend
 272 fibers are not built by stacking or piling of elements but by randomly arranged complexed polymer chains.
 273 The SAXS spectra ($I(q)$ versus q) are plotted in Figure 3 (A) in the whole SAXS range, vertically shifted for
 274 better visibility.



275

276 FIGURE 3. A) SAXS spectra of the dry crosslinked membranes (top violet: CH/CS; centre blue: CH/HA;
 277 bottom black: CH). The fitting curves are shown. The (q^{-4})-slope is observed over more than two decades. B)
 278 SAXS spectra of the crosslinked membranes after 24h immersion in DDH₂O, in the q-range corresponding to
 279 the $d < 100$ nm lengthscale (top: CH/CS; centre: CH/HA; bottom: CH). The transition from the low-q slope (q^{-4} ,
 280 see left panel) and the q^{-1} regime is clearly visible. C) SAXS spectra of the crosslinked membranes after 4-
 281 months aging in DDH₂O, in the same q-range of left panel (top: CH/CS; centre: CH/HA; bottom: CH). Spectra
 282 are shifted for better visibility.

283

284 The spectra are very similar and can be fitted with the form factor of uniform infinitely long cylinders
 285 (Pedersen, 1997) with moderate polydispersity (15%-20%), with average cross size of ~ 500 nm, compatible
 286 with the SEM observations, accounting for the variability of sample preparations. An interesting feature is
 287 that a (q^{-4})-slope is observed for all membranes over a large q-range, covering the micro-to-nanoscale,
 288 typical of objects with smooth surface. Spectra from the non-crosslinked membranes are very similar to their
 289 crosslinked analogs, indicating similar size and surface smoothness of the nanofibers (Figure S2b in SI).
 290 SAXS measurements were also performed on wet scaffolds, after 24 h immersion in distilled water. No
 291 difference is detected upon salt addition. All spectra show a clear deviation from the steep decay starting at q
 292 $\sim 3 \times 10^{-1} \text{ nm}^{-1}$, corresponding to a typical distance of ~ 20 nm, as shown in Figure 3 (B). The slope in this
 293 second regime is that of (q^{-1}), revealing the presence of additional structures on much smaller lengthscales
 294 than the fiber cross-section, with elongated shape. Those structures are conceivably polymer chains
 295 protruding and stretching out from the fibers surface.
 296 SAXS measurements were then repeated on the same membranes after 4-months aging in wet
 297 environment, to check for membrane structure evolution, reported in Fig. 3 (C). The three scaffolds

298 underwent different processes: the structure of the naked CH scaffold is preserved on both the long-range
299 and the local length-scales. The slight swelling of the fiber cross-size (~20%) indicated that hydration
300 occurred, as expected upon membrane immersion into aqueous medium, still the fibers do not unwrap or
301 disentangle or loose polymer chains. The CH/HA scaffold, instead, undergoes some structure alterations, as
302 evident from the rise of a clear shoulder in the high-q region of the spectrum, the low-q region being
303 unchanged and very similar to that of the naked CH scaffold. The shoulder could be reproduced by adding a
304 contribution coming from gaussian chains with gyration radius of 4 nm (see Fig.S2C in SI). This suggests
305 that, upon aging, longer HA chains portions (~10 monomers) protrude from the main structure, assuming a
306 coiled conformation. The deepest aging structural modification occurs in the CH/CS scaffold, (Fig. 3, C) that
307 displays changes in all the q-range. The appearance of the high-q shoulder is paralleled by a reduction of the
308 low-q slope from q^{-4} to $q^{-2.8}$, typical for a fractal structure. This is related to a more pronounced surface
309 roughening of the fibers. It seems that fibers might lose more easily some CS chains (shorter and highly
310 charged than HA and CH) probably wrapped and not intimately woven within the fibers.

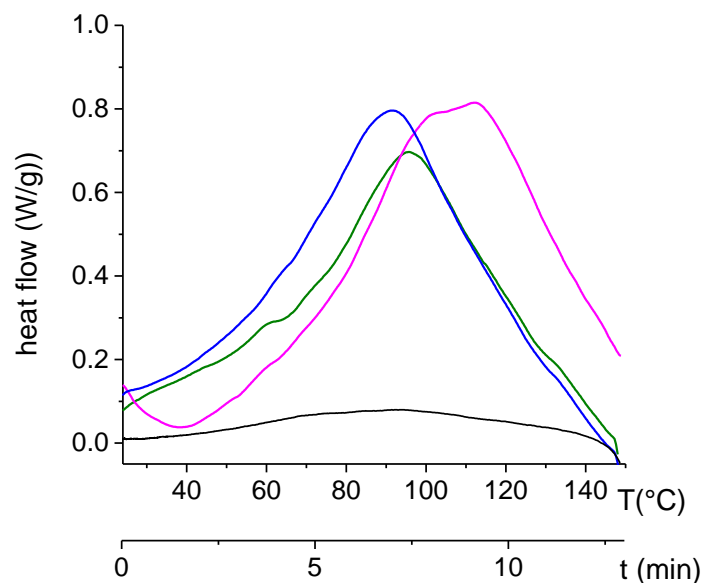
311 No differences could be highlighted after scaffold hydration in NaCl 156 mM.

312

313 3.2.4. Calorimetry

314 Calorimetry measurements were performed on non-crosslinked and crosslinked dry scaffolds, simulating the
315 cross-linking process by suddenly raising the temperature of the non-crosslinked electrospun scaffolds from
316 room up to 150°C, followed by 1-hour annealing.

317 The DSC profiles obtained with a high scan-rate (10°C/min) on non-crosslinked samples are shown in Figure
318 4. All profiles display the water-release endothermic peak (Yamaguci et al., 2001) completing below the
319 annealing temperature. The corresponding enthalpies, normalized by the sample mass to give the water-
320 holding capacity, are 244 J/g (CH), 299 J/g (CH/CS) and 279 J/g (CH/HA). The subsequent cooling to room
321 temperature and the repeated cycles are relative to annealed scaffolds in DSC-crosslinking simulated
322 protocol. No exothermic peak in the cooling scans is detected in the investigated range (Fig. 4) and no
323 water-release peak is observed in the following heating scans. Rather, the water-release peak is again
324 observed in the first DSC heating scan performed on the same samples after some delay (two weeks, two
325 and four months), showing that the scaffolds recover their hydration level in time.



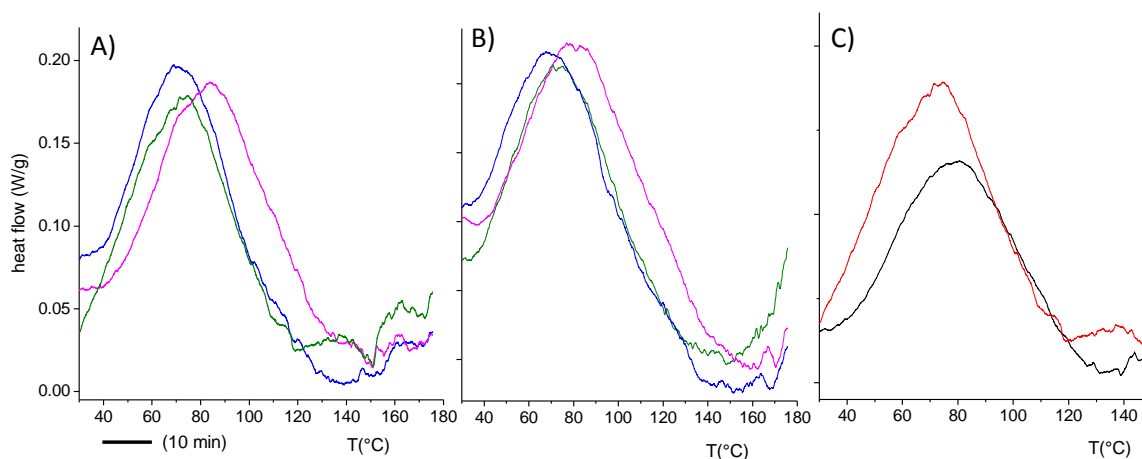
326

327 FIGURE 4. DSC-crosslinking simulation on different scaffolds with a fast (10°C/min) heating from room
 328 temperature to 150°C, of the CH (green) CH/HA (blue) and CH/CS (violet) scaffolds. In black a
 329 representative of a cooling scan. Below the temperature axis, the time axis is drawn.

330

331 Similar peaks are present in the calorigrams of the constituent materials, disappearing on closely
 332 subsequent scans and reappearing upon exposure to ambient humidity, indicating their relation to hydration.
 333 Moreover (Fig S3a in SI) the relative positions of the water-release peaks of the different scaffolds reflect the
 334 ones of their components.

335 DSC profiles of the originally-crosslinked membranes, performed at a lower scan rate of 2°C/min, are
 336 reported in Fig.5 (A). Again, the water-release peak can be clearly observed in the first heating, while it is
 337 never found in the following runs within the same experiment, as before, indicating the water-holding
 338 capacity is preserved upon crosslinking. Moreover, DSC profiles of DSC-simulated crosslinked samples
 339 (Fig.4, after two weeks), performed with the lower scan-rate of 2°C/min and shown in Fig.5 B for direct
 340 comparison, are very similar to those in left panel, stemming for good reproducibility over different samples
 341 and basic features of crosslinking. In general, the crosslinking procedure results in a downshift of the water-
 342 release temperature by ~5°C, as shown in Fig.5 C for the CH matrix, and in a higher water-holding capacity.
 343 Interestingly, a DSC-crosslinking simulation experiment performed after four months from electrospinning
 344 (Figure S3b in SI), shows that CH/CS scaffold evolution occurs also in the non-crosslinked state, as it was
 345 detected by SAXS in its crosslinked-hydrated state. The structural evolution is parallel to a modification of
 346 embedded water activity. This shows as a typical feature of the blend, which might be exploited if shorter-
 347 time membrane degradation is needed.



348

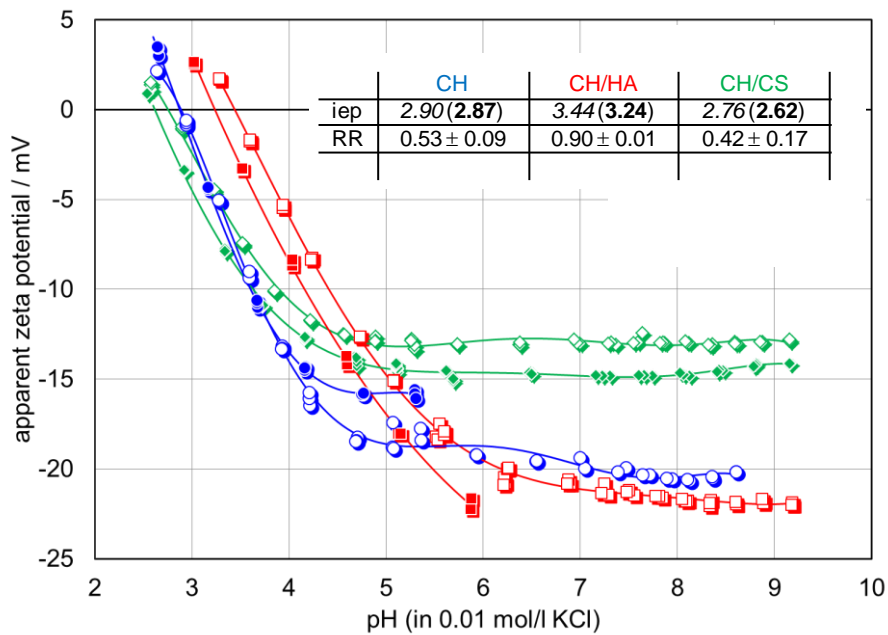
349 FIGURE 5. A) DSC of the crosslinked scaffolds, with a 2°C/min heating scan. The time scale is reported,
 350 color code as in Fig. 4. B) DSC of the DSC-simulated crosslinked scaffolds, after two weeks, with a 2°C/min
 351 heating scan. C) DSC of non-crosslinked (black) and crosslinked (red) CH scaffold.

352

353 3.2.5. Surface zeta potentials

354 Figure 6 shows the pH dependence of the ζ for the cross-linked scaffolds. The reference material is either
 355 PVDF or a silicon wafer with a SiO₂ top layer as indicated in the legend. The isoelectric points (iep) of the
 356 scaffolds are given in the inset.

357 The evolution of the apparent ζ with the pH of the aqueous 0.01 mol/l KCl solution show similar trends for CH
 358 and CH/CS scaffolds (iep at pH 2.7 ± 0.1 and at pH 2.9, respectively) and a plateau above pH 5, showing the
 359 substantial effect of CA in the CH scaffold. Nonetheless, the measured plateau values of ζ are significantly
 360 different for CH and CH/CS ($\zeta = -17.2 \pm 2.0$ mV; $\zeta = -13.8 \pm 0.9$ mV, respectively), indicating that their
 361 electric behavior at the scaffold-water interface is not the same.



362
363
364
365
366
367
368

FIGURE 6: zeta potential vs pH profiles obtained for cross-linked CH (blue), CH/CS (green) and CH/HA (red) scaffolds. In the inset, the isoelectric points (iep) of scaffolds with the two reference materials, PVDF (*italics*, full symbols) and SiO₂ (**bold**, void symbols) and the ratio RR between measured and expected Ohm resistances in the flow channel. The PVDF and SiO₂ iep are 4.02 and 3.59, respectively (SI).

369 The CH/HA scaffold displays a markedly different pH-dependence of ζ , with an iep at higher pH ($\text{pH}_{\text{iep}} 3.3 \pm$
370 0.1) and a less pronounced ζ -plateau, and only at $\text{pH} > 7.5$, a steady value of $\zeta = -22$ mV is reached.
371 Merging the information about the iep and the magnitude of the ζ in the plateau region, the three scaffolds
372 could be differentiated in terms of the surface and interfacial charge. All the three scaffolds have negative
373 zeta potential in physiological fluids, stemming for a non-negligible impact of CA 1:1 in weight ratio to
374 chitosan, otherwise expected to show a much higher iep. However the different behavior of the three
375 scaffolds, considering iep and ζ at plateau regions, could be related to the strong interaction between CS
376 and the amino groups of CH that could compete with CH-CA interaction, while the interaction between CH
377 and HA is conceivably weaker considering the lower acidity of the carboxylic groups of HA as compared to
378 the sulfate groups of CS. Combined measurement of streaming potential and streaming current (detailed in
379 SI) allowed estimating the ratio (RR, Fig 6, inset) of the effective and electrolyte resistances (RR). CH and
380 CH/CS scaffolds are characterized by similar low values of RR (0.53 ± 0.09 and 0.42 ± 0.17 , respectively),
381 which indicate a significant effect of swelling. The RR value close to unity (0.90 ± 0.01) for CH/HA suggests
382 that this shows a smaller swelling propensity. The apparently contrasting information about the swelling
383 propensity of the different scaffolds as determined by microscopy, SAXS and ζ , shows that swelling occurred

384 at different scales. In fact, it appears that in the CH/HA scaffold swelling is sustained by single fibers, while in
385 the CH and CH/CS, it is due to dilatation of the scaffold mesh.

386

387 3.2.6. Mechanical properties

388 Both dry and hydrated cross-linked scaffolds were tested for tensile strength TS (N/cm^2) and elongation (E%)
389 at break point (Fig. S5, SI). All scaffolds display higher TS and lower E% in dry rather than wet state (both
390 parameters, by roughly one order of magnitude). When dry, CH/CS TS value is roughly half than for CH and
391 CH/HA, with similar elongation. In the hydrated state, this feature is more evident, as, although showing
392 similar values of force at break, CH/CS scaffold shows significantly higher values for E%, roughly doubling its
393 length before breaking, about 20% higher than the CH scaffold and twice that of CH/HA. Then, the presence
394 of CS conceivably improves the ability of the scaffold to be deformed without breaking.

395

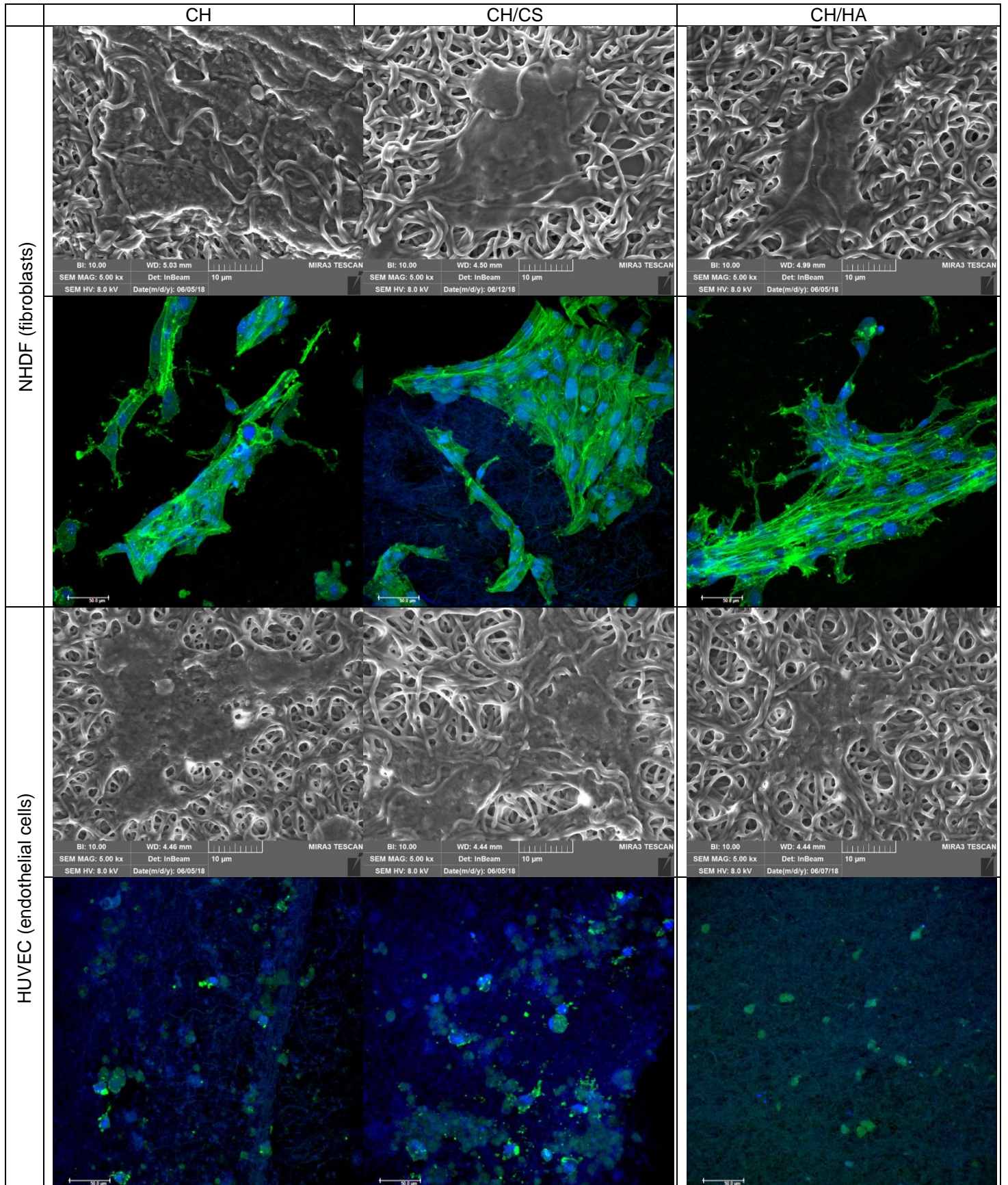
396 3.3. Biopharmaceutical characterizations

397 3.3.1. In vitro cell adhesion and proliferation assay: fibroblasts and endothelial cells

398 In Figure S6 cytotoxicity results are shown and fibroblasts and HUVEC viability (optical density, OD)
399 evaluated for cells grown onto CH, CH/CS and CH/HA scaffolds and in standard conditions (GM, cells grown
400 directly on plastic well bottom was considered as standard growth) for 3 and 6 days is reported (SI).
401 Independently of the cell type there is an increase in cell population grown onto scaffolds from 3 to 6 days to
402 indicate that the scaffolds support the cell growth along time without impairing their proliferation and no
403 difference between GM and scaffolds could be evidenced.

404 While after 6 days fibroblasts proliferate much more onto CH/CS scaffolds while CH scaffolds is
405 characterized by lower cell proliferation than GM. In the case of HUVEC, scaffolds allow a cell growth like
406 GM: CH/HA determined a cell growth higher than those of the other scaffolds and CH/CS showed a slightly
407 lower cell proliferation with respect to CH/HA.

408 Figure 7 reports SEM and CLSM of fibroblasts (a) and HUVEC (b) grown onto scaffolds for 6 days (the 3
409 days growth is shown in Fig. S7). These analyses confirm the proliferation results (viability). SEM
410 microphotographs evidence that cells grow in an intimate contact with the scaffold structure and the
411 nanofibers appear integrated in the cell substrates at subconfluency. CLSM put in evidence that fibroblasts
412 grown onto the scaffolds are characterized by normal fusiform shapes and aligned cytoskeletons while
413 HUVEC cells present polygonal shape. CH and CH/CS scaffolds seem to better allow cell adhesion and
414 proliferation showing greater number of cells.



415 FIGURE 7: SEM and CLSM (in blue the nuclei and in green the cytoskeleton) microphotographs of
 416 fibroblasts (NHDF) and endothelial cells (HUVEC) grown onto CH (left), CH/CS (centre) and CH/HA (right)
 417 scaffolds for 6 days.

418 3.3.2. In vivo wound healing efficacy in rat model

419 Figure 8 shows lesion area vs time of treatments and the histology in correspondence of the lesions after 18
420 days of treatment with CH, CH/CS and CH/HA scaffolds in an in vivo murine burn/excisional model. Intact
421 skin (positive reference) and skin section in correspondence to the lesion after 18 days of treatment with
422 saline solution (negative reference) are also reported.

423 Lesions treated with CH/CS, CH and CH/HA are in a more advanced stage of wound healing as compared to
424 samples treated with saline solution (Fig. 8 B), in which there is a large part of skin surface without
425 epithelium. Furthermore, in saline-treated lesions, the underlying connective tissue is still affected by an
426 abundant inflammatory infiltrate, with numerous dilated vessels, while collagen fibers are dispersed and not
427 yet organized. All the scaffolds can improve the skin recovery as compared to the reference although there
428 are differences in scaffold performance. CH/CS appears to be the best performing of the three (Fig. 8 D).
429 The epidermal layer appears fully restored, thick and well organized in several cell layers, and shows a fair
430 degree of keratinization (cornification). Inflammatory infiltrate is almost completely absent, as well as
431 abnormally dilated vessels. A fine network of collagen fibers is restored at the dermo-epidermal junction and
432 the bundles of collagen fibers in the dermis has a normal size.

433 CH scaffold (Fig. 8 C) shows full restoration of the epidermal layer, thick and fairly keratinized. Bundles of
434 collagen fibers of normal size are restored at the wound edges. But the dermis in the injured area is still
435 rather infiltrated by inflammatory cells with several dilated vessels. Finally, also the CH/HA scaffold (Fig. 8
436 E) displays a suboptimal performance with the epidermal layer not fully restored, and necrotic material
437 detectable over the lesion. The dermis in the injured area is infiltrated by several inflammatory cells with
438 dilated vessels.

439 In all cases the histologic analysis does not show any residues of the scaffolds. This could be probably due
440 to enzymatic degradation caused by lysozyme, which chitosan is a substrate of. In fact lysozyme is normally
441 secreted by white cells recruited in the lesion bed during the inflammatory phase of the healing process.

442

443

444

445

446

447

448

485 Conclusions

486 Electrospinning was successfully used to prepare scaffolds for reparation of critical skin lesions, like burns.
487 The developed process allowed to obtain nanofibrous membranes entirely based on polysaccharides,
488 starting from aqueous polymer blends. Polymers with opposite charges (CH, cationic, and CS or HA, anionic)
489 could be simultaneously electrospun with P as matrix-forming polysaccharide. CA, present in the polymer
490 blends, was added as cross-linking agent and activated by heating.

491 The nanofibers show regular shape and smooth surface, preserved upon the cross-linking process. The
492 resistance of scaffolds to solubilization in aqueous fluids seems attributable to two phenomena occurring at
493 crosslinking heat treatment: the creation of amide bonds (mainly in the CH scaffold, while hindered by the
494 formation of PEC in CH/CS and CH/HA scaffolds) and felting, occurring when water is released from the
495 electrospun scaffold, resulting in local physical multi-entanglement between fibers, that could not be released
496 by simple hydration. Nonetheless, the water holding capacity of the scaffolds is preserved, and conceivably
497 increased, by crosslinking,

498 CH/CS scaffold shows the best performance in allowing the skin healing in vivo (murine burn/excisional
499 model) and correspondingly, it evidences the best proliferation properties in vitro (fibroblasts and HUVEC).

500 The physico-chemical analysis suggests that the CH/CS scaffold offers more adaptability in terms of swelling
501 and fiber roughening once hydrated, thus conceivably allowing for optimal cell adhesion and migration,
502 moreover profiting from the CS protrusion/release from the fibers. In addition, the macroscopic feature of a
503 pronounced deformability pointed at the CH/CS scaffold as a good protective cover for non-flat or irregular
504 surfaces.

505

506 Acknowledgements

507 The authors thank M. Sztucki for assistance on ID02 (ESRF, Grenoble) and the partnership for Soft
508 Condensed Matter (PSCM, ILL/ESRF, Grenoble) for use of in-house facilities.

509

510 Funding

511 This research did not receive any specific grant from funding agencies in the public, commercial, or not-for-
512 profit sectors.

513

514 Data availability

515 The raw and processed data required to reproduce these findings cannot be shared at this time as part of an
516 ongoing study. In the SI supplementary findings support the results obtained.

517

518 REFERENCES

519 Feng, F., Liu, Y., Zhao, B., Hu, K. (2012) Characterization of half N-acetylated chitosan powders and films,
520 *Procedia Engineering*, 27, 718-732.

521 Goldberg, M., Langer, R., Jia, X. (2012) Nanostructured materials for applications in drug delivery and tissue
522 engineering, *Journal of Biomaterials Science Polymer edition*, 18, 241-268.

523 Harish Prashanth, K.V., Kittur, F.S., Tharanathan, R.N. (2002) A physico-chemical comparative study on
524 extracellular carbohydrate polymers from five desert algae, *Carbohydrate Polymers*, 50, 27-32.

525 Huan, S., Liu, G., Han, G., Cheng, W., Fu, Z., Wu, Q., Wang, Q. (2015) Effect of Experimental Parameters
526 on Morphological, Mechanical and Hydrophobic Properties of Electrospun Polystyrene Fibers. *Materials*, 8,
527 2718 -2734

528 Kim, H., Jeong, H., Han, S., Beack, S., Hwang, B. W., Shin, M., Oh, S. S., Hahn, S. K. (2017) Hyaluronate
529 and its derivatives for customized biomedical applications, *Biomaterials*, 123, 155-171.

530 Kupiec, T.C., Matthews. P., Ahmad, R. (2000) Dry-heat sterilization of parenteral oil vehicles. *International*
531 *Journal of Pharmaceutical Compounding*, 4, 223-4.

532 Liu, H., Wang, C., Li, C., Qin, Y., Wang, Z., Yang, F., Li, Z., Wang, J. (2018) A functional chitosan-based
533 hydrogel as a wound dressing and drug delivery system in the treatment of wound healing, *RSC Advances*,
534 8 7533-7549.

535 Liu, M., Duan, X.-P., Li, Y.-M., Yang, D.-P., Long, Y.-Z. (2017) Electrospun nanofibers for wound healing,
536 *Materials Sciences and Engineering C*, 76, 1413-1423.

537 Luxbacher, T. (2014) The ZETA Guide – Principles of the streaming potential technique, Anton Paar GmbH,
538 ISBN 978-3-200-03553-9

539 Mafazzal Jahromi, M.A., Sahandi Zangabad, P., Moosavi Basri, S.M., Sahandi Zangabad, K., Ghamarypour,
540 A., Aref, A.R., Karimi, M., Hamblin, M.R. (2018) Nanomedicine and advanced technologies for burns:
541 Preventing infection and facilitating wound healing, *Advanced Drug Delivery Reviews*, 123, 33-64.

542 Oliveira, J. T., Reis, R. L.J. (2011) Polysaccharide-based materials for cartilage tissue engineering
543 applications, *Tissue Engineering and Regenerative Medicines*, 5, 421 -36.

544 Pedersen, J. S. (1997) Analysis of small-angle scattering data from colloids and polymer solutions: modeling
545 and least-squares fitting *Advances in Colloid and Interface Sciences*, 70, 171-210

546 Qasim, S.B., Zafar, M.S., Najeeb, S., Khurshid, Z., Shah, A.H., Husain, S., Rehman I. U. (2018)
547 Electrospinning of Chitosan-Based Solutions for Tissue Engineering and Regenerative Medicine,
548 *International Journal of Molecular Sciences*, 19, 407.

549 Sandri, G., Bonferoni, M. C., Rossi, S. Ferrari, F., Mori, M., Cervio, M., Riva, F., Liakos, I., Athanassiou, A.,
550 Saporito, F., Marini, L., Caramella, C. (2015) Platelet lysate embedded scaffolds for skin regeneration,
551 *Expert Opinion on Drug Delivery*, 12, 525-545. <https://doi.org/10.1517/17425247.2015.961421>.

552 Sandri, G., Bonferoni, M. C., Rossi, S., Delfino, A., Riva, F., Icaro Cornaglia, A., Marrubini, G., Musitelli, G.,
553 Del Fante, C., Perotti, C., Caramella, C., Ferrari, F. (2016) Platelet lysate and chondroitin sulfate loaded
554 contact lenses to heal corneal lesions, *International Journal of Pharmaceutics*, 509, 188-196.

555 Sandri, G., Bonferoni, M. C., Rossi, S., Ferrari, F., Mori, M., Del Fante, C., Perotti, C., Caramella, C. (2012)
556 Thermosensitive eyedrops containing platelet lysate for the treatment of corneal ulcers *International Journal*
557 *of Pharmaceutics*, 426, 1-6.

558 Saporito, F., Sandri, G., Rossi, S., Bonferoni, M.C., Malavasi, L., Del Fante, C., Vigani, B., Black, L., Ferrari,
559 F. (2018a) Electrospun gelatin–chondroitin sulfate scaffolds loaded with platelet lysate promote immature
560 cardiomyocyte proliferation. *Polymers*, 10, 208.

561 Saporito, F., Sandri, G., Rossi, S., Bonferoni, M.C., Riva, F., Malavasi, L., Caramella, C., Ferrari, F. (2018b)
562 Freeze dried chitosan acetate dressings with glycosaminoglycans and traxenamic acid, *Carbohydrate*
563 *Polymers*, 184, 408-417.

564 Singh, R.S., Kaur, N., Rana, V., Kennedy, J.F. (2017) Pullulan: A novel molecule for biomedical applications
565 *Carbohydrate Polymers*, 171, 10-121.

566 Stejskalova, A., Almquist, B.D. (2017) Using biomaterials to rewire the process of wound repair, *Biomaterials*
567 *Science*, 5, 1421- 1434.

568 Walker, S. L., Bhattacharjee, S., Hoek, E. M. V., Elimelech, M. (2002) A Novel Asymmetric Clamping Cell for
569 Measuring Streaming Potential of Flat Surfaces. *Langmuir*, 18, 2193 –2198. DOI: 10.1021/la011284j

570 Yamada, S., Sugahara, K. (2008). Potential therapeutic application of chondroitin sulfate/dermatan sulfate,
571 *Current Drug Discovery. Technologies*, 5, 289-301

572 Yamaguchi, I., Tokuchi, K., Fukuzaki, H., Koyama, Y., Takakuda, K., Monma, H., Tanaka, J. (2001)
573 Preparation and microstructure analysis of chitosan/hydroxyapatite nanocomposites, *Journal of Biomedical*
574 *Material Research*, 55, 20-27.

Supplementary data

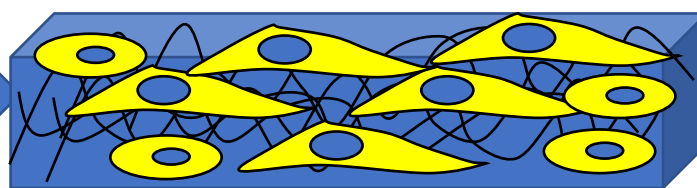
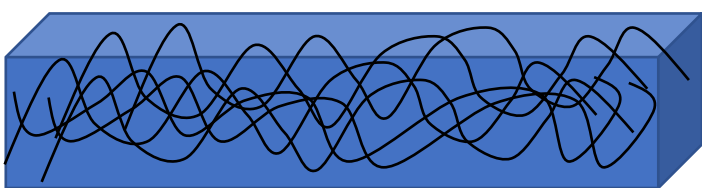
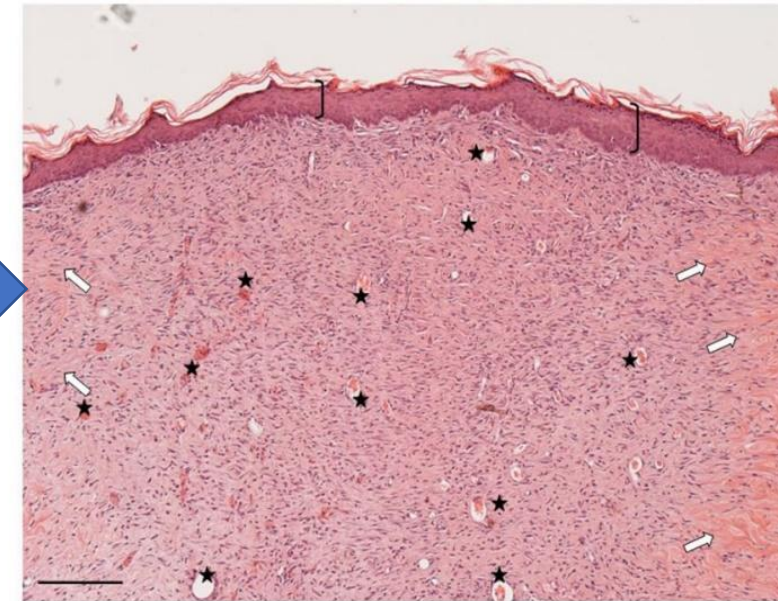
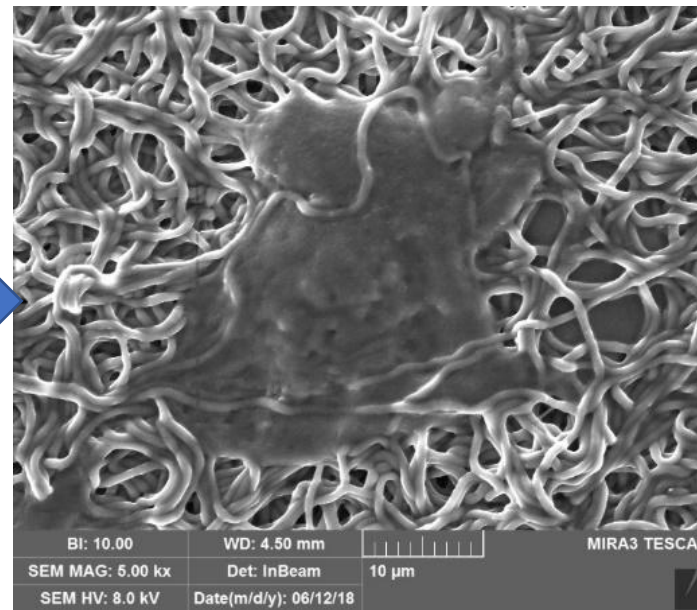
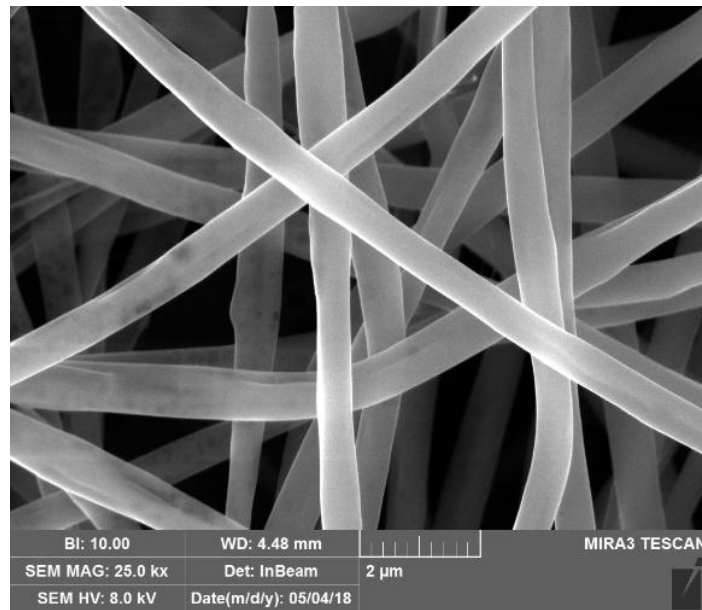
[Click here to download Supplementary data: CB SI R.docx](#)

Graphical Abstract

**Polysaccharide based
electrospun scaffolds**

**In vitro fibroblasts and endothelial cells
adhesion and proliferation**

**In vivo (murine burn/excisional model)
skin reparation**



**Scaffold based on
chitosan/chondroitin sulfate**

